Materials Research Express

OPEN ACCESS

RECEIVED
18 May 2021

REVISED
9 August 2021

ACCEPTED FOR PUBLICATION
22 October 2021

PUBLISHED
10 March 2023

PAPER

Structural, thermal and optical studies of Eu3+ ion doped $Ge_{22}As_{20}Se_{58}$ glass

Amarendra Kumar Singh[1,*], **Neeraj Mehta**[1], **Hirdeysh Mishra**[1] and **S K Mishra**[2]

[1] Department of Physics, Banaras Hindu University, Varanasi, Uttar Pradesh, India
[2] Instruments Research & Development Establishment (DRDO), Dehradun, Uttarakhand, India
* Author to whom any correspondence should be addressed.

E-mail: amarendra124@gmail.com

Keywords: chalcogenide glass, infrared imaging, luminescent, amorphization, absorbance

Abstract

The effect of Eu^{3+} doping on improving the amorphous nature of commercial chalcogenide glass/ChG ($Ge_{22}As_{20}Se_{58}$), which is typically used as a molded lens for mid-infrared imaging, has been investigated. The observed absence of bright spots in Transmission Electron Microscope-Selected area (electron) diffraction (TEM-SAED) pattern confirmed the doping-induced amorphous nature of Eu-$Ge_{22}As_{20}Se_{58}$ glass. The thermal studies over glass transition temperature (Tg) using DSC technique also revealed that Eu doping has increased the amorphous nature along with the thermal stability of $Ge_{22}As_{20}Se_{58}$ glass. The optical analysis using UV–vis absorption spectroscopy showed that the activity of Eu-doped ChG has been extended across the UV-visible region. Tauc plot derived band gap energy of Eu-doped and undoped ChG is found to be 2.2 and 2.6 eV, respectively.

List of abbreviations

XRD	X-Ray Diffraction
TEM-SAED	Transmission Electron Microscope- Selected area (electron) diffraction
ChG	Chalcogenide glasses
DSC	Differential Scanning Calorimetric
FSDP	First Sharp Diffraction Peak
SEM	Scanning electron microscope
MWIR	Medium Wavelength Infrared
LWIR	Long Wavelength Infrared

1. Introduction

In recent years, rare-earth doping in chalcogenide glasses (ChG) leads to interesting and promising enhancements in their optical properties in the near- and mid-infrared regions [1]. ChG with a composition of $Ge_{22}As_{20}Se_{58}$ is a commercially important molded optical lens and is active in MWIR (3–5 μm) and LWIR (8–12 μm) regions, which is extensively used for infrared imaging, low loss optical fiber, and thermal screening applications. However, lower thermal stability of ChG leads to aberrations in the lenses and eventually limits its applications. Thus, there is a need to perform suitable modifications in their chemical compositions [2]. In this direction, it is observed that rare-earth doping enhances the thermal stability as well as overall optical properties of ChGs. Accordingly, there have been many works reported on rare-earth doped ChG systems [3]. Yong, *et al*, have studied the effect of Pr^{3+} doping on the luminescent property of Ge-Sb-Se glass. From the calculated radiative and non-radiative transition rates, it was proposed that the emergence of radiation-less energy transfer between Pr 4 f energy levels and host could be due to the electric multipole-multipole interactions, which

ultimately enhanced the luminescent properties of Pr-doped Ge-Sb-Se glass [4]. Similarly, Li, *et al*, have prepared Er^{3+} and Pr^{3+} ions-doped Ga-Sb-S ChG by melt-quenching method [5]. In this study, they observed the energy transfer from Er^{3+} and Pr^{3+} within the host at an excitation wavelength of 808 nm, where they observed that the emission at 1550 nm corresponding to Er^{3+} was reduced, while the emission at 2740 nm corresponding to Pr^{3+} was increased. On the other hand, Abdellaoui, *et al*, prepared ChG with a complex structure consisting of $Ga_5Ge_{20}Sb_{10}Se_{(65-x)}Te_x$ (x = 0, 10, 20, 25, 30, 32.5, 35, 37.5) and studied its application as an optical fiber, in which 500 ppm of Tb^{3+} was doped in $Ga_5Ge_{20}Sb_{10}Se_{65}$ and $Ga_5Ge_{20}Sb_{10}Se_{45}Te_{20}$ glass [6]. From the Judd-Ofelt calculations, the lifetime of 8.9 and 7.8 ms was estimated for selenide and seleno-telluride matrix, respectively, during radiative transition from $^7F_5 \rightarrow {}^7F_6$ in the range of 4.3–6.0 μm. A review by Sujecki highlighted the characteristics of MIR sources, low-cost laser sources based on ZBLAN fiber and rare-earth (Pr^{3+}, Dy^{3+}, Tb^{3+})-doped ChG-based MIR fiber laser cavity designs [7]. Interestingly, Shiryaev *et al* conducted experimental and numerical studies on the emission properties of Pr^{3+} doped Ga(I)-Ge-As-Se glass fibers [8]. Churbanov *et al* synthesized the Pr^{3+} doped $Ge_{36}Ga_5Se_{59}$ glass at different concentrations. The obtained results demonstrated that the doped $Ge_{36}Ga_5Se_{59}$ glass showed luminescence in the range of 1.6–7.5 μm [9]. For the first time, Starecki *et al* reported the luminescence emission in LWIR ($^6H_{7/2} \rightarrow {}^6H_{9/2}$ transition) at 7.3 μm wavelength in 1000 ppm Dy^{3+}-doped $Ga_5Ge_{20}Sb_{10}Se_{58}$ glass [10].

Recently, Kilic *et al* [11] prepared zinc-borate glass with a chemical composition of (100-x)-($60ZnO{\cdot}40B_2O_3$)-xEu_2O_3 and studied the optical and radiation shielding characteristics of the glass with respect to increasing mol% of Eu_2O_3 from 0 to 3%. The band gap energy of the glass was decreased from around 4.47 eV to 3.36 eV at 3 mol% Eu_2O_3; the same materials also showed the highest radiation shielding properties. Accordingly, it is suggested that the increasing concentration of Eu_2O_3 directly influences the glass nature of the system, and thereby, it possessed superior properties as compared to pristine glass. Similarly, Naseer *et al* [12] studied the impact of Bi_2O_3 as a modifier agent on barium-zincborate (BZX) glasses towards improving their radiation-shielding properties. The BZX glasses were prepared using the melt-quenching method and studied for their structural and elastic characteristics associated with the radiation-shielding properties. The 15% Bi_2O_3 BZ glass exhibited the maximum sound-resistant properties, whereas the highest mass and linear attenuation coefficient values and shielding effect were observed in BZ30 glass. It was proposed that the increasing concentration of Bi^{3+} in the host glass system augmented the BO_4 units and bonds in metal-oxides, and thereby, it improved the overall stability of the glass material. Further, it was also claimed that Bi_2O_3 introduced in the glass matrix acted as a network former/modifier in the composition. Accordingly, the observed decreased elastic moduli values proved that there could be an elevated cross-linking density in the system due to the incorporated Bi_2O_3. In addition, the estimated values of fractional dimension suggested that the glass network was changed from 2D to 3D network due to the presence of Bi_2O_3 modifier in the host BZX glass.

To this end, this work reports the effect of rare-earth Eu^{3+} ions doping in the commercial $Ge_{22}As_{20}Se_{58}$ ChG towards enhancing its amorphous nature and optical properties via the doping-induced amorphization process. It should be noted that the amorphization is responsible for tuning the mid-IR transmission properties in $Ge_{22}As_{20}Se_{58}$ glass. The obtained results from various structural investigations such as XRD, Raman and ATR-IR indicate that Eu doping essentially breaks down the crystalline network and increases amorphous nature in the system. Similarly, the SEM and TEM images showed the doping-induced changes in the morphology of the material. Interestingly, the absence of bright spots in the TEM-SAED pattern of Eu-doped ChG indicated the manifestation of enhanced amorphous nature in the material. Thermal studies using DSC revealed the enhanced amorphous nature and thermal stability in the glass. Further, the UV-visible absorption spectrum showed that the doped ChG possessed enhanced activity in the visible and near-IR regions as compared to the non-doped ChG.

2. Methods

Commercial $Ge_{22}As_{20}Se_{58}$ glass was used in this study, and rare-earth doping was carried out by melt quenching method without using gallium. From the literature, an optimized value of 3% was selected. Accordingly, 3% of Eu_2O_3 was doped in the $Ge_{22}As_{20}Se_{58}$ glass. In this process, initially, the required amount of glass powder and Eu_2O_3 precursor were taken in a quartz ampoule under 10^{-5} torr pressure in order to remove any oxidant gases present, and then it was kept in a furnace and heated to 873 K at a heating rate of 2 °C/min and kept in it for 10 h. In order to ensure the homogeneous thermal distribution, the sample mixture was shaken every five minutes, and finally, it was rapidly quenched by keeping it in an ice bath after completing the heating process. Then, the ampoule was crushed to get the glass sample in powder form.

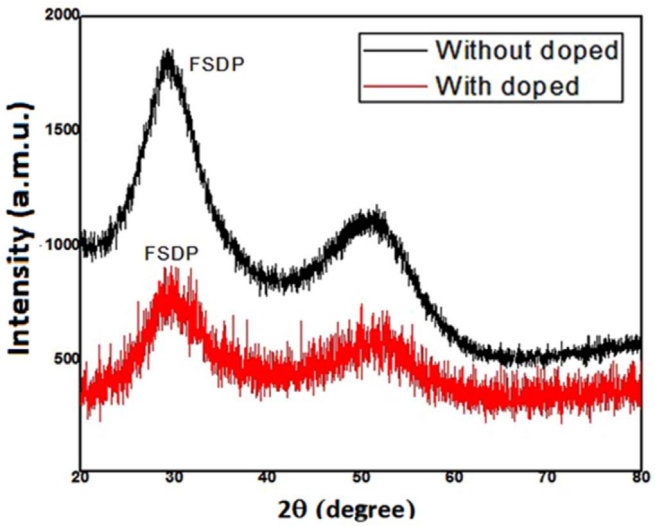

Figure 1. XRD-spectrum of undoped and 3% Eu-doped $Ge_{22}As_{20}Se_{58}$ glass.

Table 1. XRD-result for with and without Eu^{3+} ions $Ge_{22}As_{20}Se_{58}$ glass.

Glass	2θ(°)	FWHM(°)	Q_1(Å^{-1})	ΔQ_1(Å^{-1})	R(Å)	L(Å)
Ge_{22} As_{20} Se_{58}	29	6.81	2.04	0.48	3.10	13.10
Ge_{22} As_{20} Se_{58}-Eu (3%)	30	8.19	2.11	0.58	2.98	10.83

3. Results and discussion

3.1. Structural characterizations

XRD pattern of the pristine and Eu-doped ChG is given in figure 1.

It is clear from the obtained XRD pattern that Eu doping has substantially induced the amorphous nature in the host ChG. Eu doping essentially breaks down the long-range crystalline network into short-range orders, which induces more amorphous nature in the material. This occurs due to the predominant interaction of Eu ions with Se ions as they have been doped in the sites of Se. It should also be noted that Se ions are relatively more volatile within the structure of $Ge_{22}As_{20}Se_{58}$ glass. As it is the major constituent in the system, the influence by Eu doping at the sites of Se leads to disorders in the matrix of $Ge_{22}As_{20}Se_{58}$ glass, which eventually induces more amorphous nature in the material [10]. Fist peak is first order diffraction, and second peak is second order diffraction.

The Elliott void-cluster model can be applied to investigate the glassy materials with tetrahedral structural units, where it proposes that the glassy nature occurs in the material due to the separation of the group of atoms or clusters by voids or regions with certain atomic densities [13]. Accordingly, in figure 1, the semi-crystalline nature of $Ge_{22}As_{20}Se_{58}$ glass can be understood from the observed lower full-width ad half-maximum (FWHM) value of the first sharp diffraction peak (FSDP).

Considering that the incident wavelength (λ) of the X-ray is 1.54 Å, diffraction peak at 2θ, FWHM showing the broadness of the peak, Q_1 is the magnitude of scattering vector, ΔQ_1 magnitude of scattering vector in FWHM, R is the effective periodicity and L is the correlation length, the glassy nature of the materials can be obtained and correlated with various parameters of FSDP [14]. These parameters include magnitude of the scattering vector $Q_1 = 4\pi\sin\theta/\lambda$, interlayer separation quasi-periodic in nature with an effective periodicity $R \approx 2\pi/Q_1$ and correlation length $L \approx 2\pi/\Delta Q_1$ as shown in table 1. These observed increased values of FSDP parameters corresponding to Eu-doped $Ge_{22}As_{20}Se_{58}$ glass (table 1) clearly showed that the amorphous nature of the system is increased due to Eu doping.

The TEM (Transmission electron microscope) and SEM (Scanning electron microscope) images of both pristine and Eu-doped $Ge_{22}As_{20}Se_{58}$ glasses are displayed in figures 2(a)–(d) and the SAED patterns are given in the insert of figures 2(a) and (b), respectively.

These obtained images showed substantial differences in both the surface morphology as well as the internal structure of the samples, which can be attributed to the Eu doping-induced effects in the materials. It can be seen that the smooth surface and interior structure of pristine ChG is turned into rough and matrix-like structure in

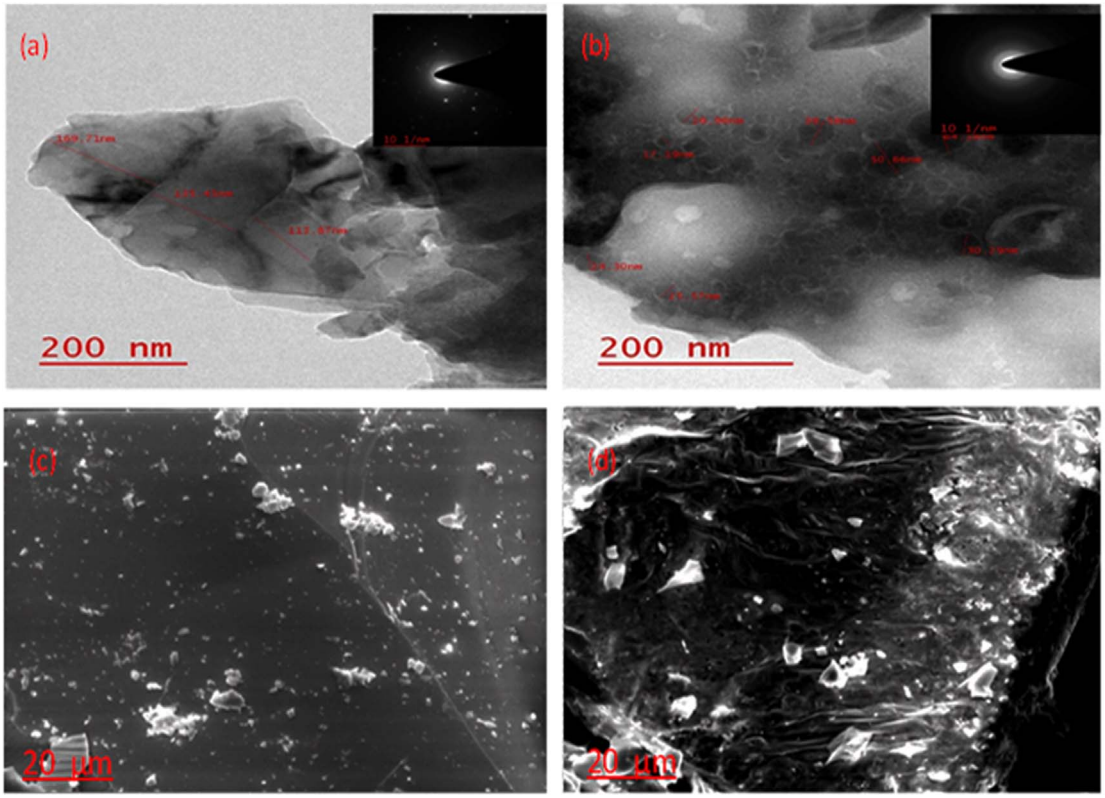

Figure 2. TEM image and SEM image of (a) undoped $Ge_{22}As_{20}Se_{58}$ glass with semi-crystalline glassy nature; (b) 3% Eu^{3+} ions doped $Ge_{22}As_{20}Se_{58}$ glass showing the glassy nature; (c) SEM image of the undoped $Ge_{22}As_{20}Se_{58}$ glass; (d) SEM of 3% Eu-doped $Ge_{22}As_{20}Se_{58}$ glass.

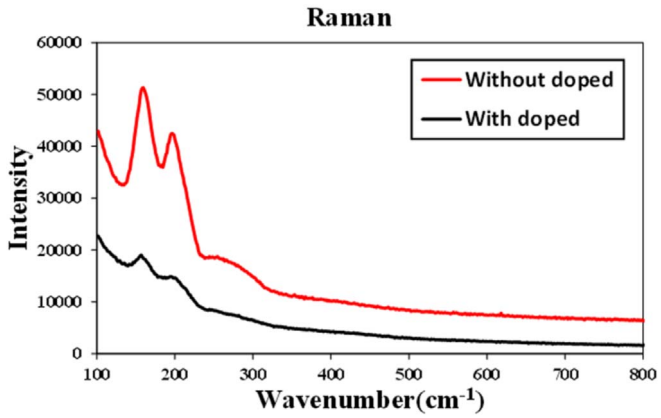

Figure 3. Raman spectrum of undoped and 3% Eu-doped $Ge_{22}As_{20}Se_{58}$ glass.

the case of doped-ChG, which could be ascribed to the emerged amorphous nature in host ChG. Furthermore, the absence of bright spots in the obtained TEM-SAED patterns (insert images of figures 2(a)–(b)) clearly revealed that the crystalline nature of the host $Ge_{22}As_{20}Se_{58}$ glass is greatly suppressed upon Eu doping [15].

The doping-induced structural changes in Eu-doped ChG were investigated using Raman spectroscopy, and the obtained spectra are displayed in figure 3.

From the Raman spectrum of the pristine ChG, the broad peak at 285–300 cm^{-1} could be assigned to the asymmetric-vibration mode of $GeSe_4$ structure. Similarly, the peak at 265 cm^{-1} is A_1 mode of corner linked dimer's small Se_n chains [$GeSe_{4/2}$]. The peak in the range of 240–250 cm^{-1} is A_1 mode of Se_n ring, where the peak at 245 cm^{-1} indicates stretching modes of Se-Se at the outer trigger, and the peak at 235 cm^{-1} is A_1 mode of Se_n chains in the –Se links. The band at 215 cm^{-1} can be assigned to A_1 breathing companion mode of $GeSe_{4/2}$ connected by the edges, and the band at 200 cm^{-1} is A_1 sym stretching mode of $GeSe_{4/2}$ connected by the

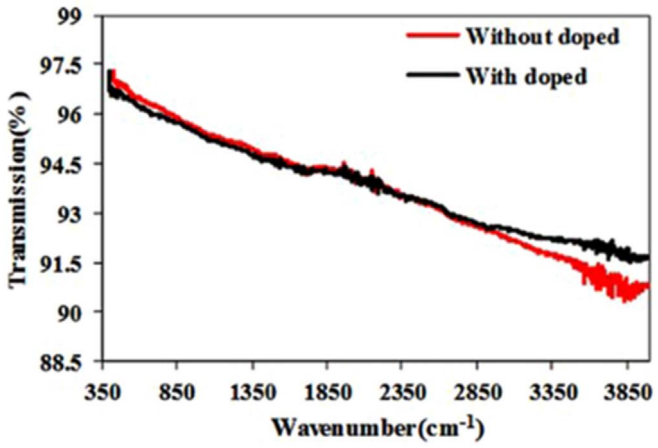

Figure 4. ATR- FTIR spectrum of undoped and 3% Eu-doped $Ge_{22}As_{20}Se_{58}$ glass.

corners. Furthermore, the band at 190 cm^{-1} can be assigned to stretching of As-Se bonds, the peak at 155 cm^{-1} can be assigned to Se_2As-$AsSe_2$, and the peak at 145 cm^{-1} could be due to Se-Se at the outer trigger. The 138 cm^{-1} peak could be assigned to the rotational vibration mode of Se polymetric chain [16, 17]. On the other hand, these observed Raman peaks are significantly suppressed and deformed in the case of Eu-doped ChG. This indicates that the doping of Eu causes severe structural changes in the host ChG, which could be directly attributed to the reduced crystalline nature in the system. As discussed, the appearance of major peaks in the Raman spectrum of pristine ChG is largely due to Se, which is the key site to induce the amorphous nature in ChG system as well. Accordingly, the suppressed peaks in the Raman spectrum of doped ChG could be assigned to doping-induced amorphization via structural deformation in the crystalline network of the host ChG [16, 17].

The ATR-IR spectra of the samples, as displayed in figure 4, hardly showed any difference, which indicated that Eu doping in ChG did not lead to any changes in the surface functional groups of the samples. However, the peaks in the region 3500–4000 cm^{-1} corresponding to the adsorbed moisture on surface were found to be drastically decreased. This indicates that Eu-doping creates a resistive layer for the moisture adsorption, which may eventually contribute to enhancing the optical properties of ChG [18].

3.2. Thermal stability analysis

The amorphous nature of glass can be clearly assessed by the mean bond energy of a covalent network in the glass, which is associated with its glass transition temperature (T_g). It should be noted that glass transition kinetic is dependent of the glass transition temperature (Tg) and activation energy (Eg). Therefore, the differential scanning calorimetric (DSC) analysis of pristine and Eu-doped ChG was carried out at different heating rates, and the obtained data are displayed in figures 5(a)–(b).

From the obtained DSC curves, the observed two glass transition temperatures essentially indicated that the $Ge_{22}As_{20}Se_{58}$ glass has two molecular structures as the Se network is highly reticulated by the trivalent As (As_2Se_3) and tetravalent Ge ($GeSe_4$) structure, which can be corroborated with their Raman spectra as well [19, 20]. Accordingly, the glass transition takes place at Tg in the case of pristine $Ge_{22}As_{20}Se_{58}$ glass (figure 5(a)), while it is greatly affected in the case of Eu-doped $Ge_{22}As_{20}Se_{58}$ glass (figure 5(b)) due to its established amorphous nature. This signifies that when this glass is heated above this Tg, the material will become vicious and will not show any further crystallization tendency, and therefore, it becomes suitable for molding optics under moderate pressure [19]. For instance, figure 6 shows some of the sophisticated infrared optics including aspheric and asphero-diffractive lenses, which can be directly inserted into a thermal imaging system such as an infrared camera. In general, glass materials based on silicon, germanium and chalcogenides ($Ge_{22}As_{20}Se_{58}$) are used in such infrared cameras [21].

In addition, the Tg and Ts (solidification temperature) play an important role in optical molding [22]. As shown in figures 5(a)–(b), there is no proper crystalline peak observed for Eu-doped ChG under the given temperature range ΔT, where $\Delta T = Ts—Tg$, which can be defined as the temperature difference between Ts and Tg. Notably, ΔT is often considered a criterion to measure thermal stability and glass forming ability of the materials. Larger ΔT essentially means the better inhibition of crystallization process. Therefore, glass should have a high ΔT value, which will essentially enhance the scattering loss in optical fibers. Ideally, ΔT should be greater than 120 °C to minimize the possibility of crystallization.

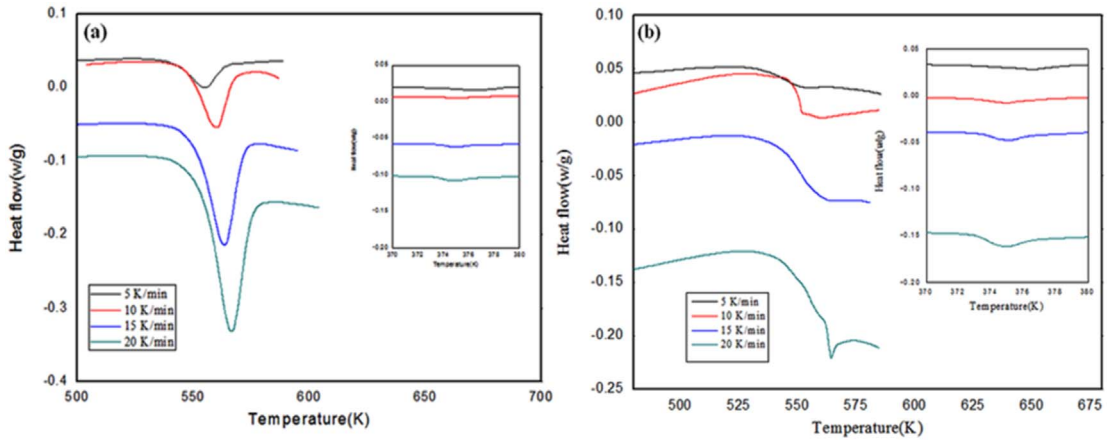

Figure 5. DSC heat flow at the different rates of 5, 10, 15 and 20 K min^{-1}: (a) undoped and (b) 3% Eu doped $Ge_{22}As_{20}Se_{58}$ glass.

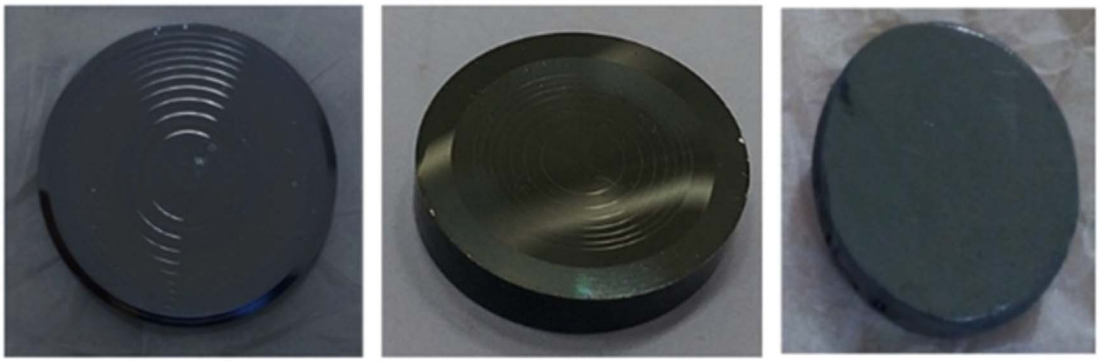

Figure 6. Asphero-diffractive optics by SPDT (Single Point Diamond Turning) machining on silicon, germanium, without machining chalcogenide glass ($Ge_{22}As_{20}Se_{58}$) in bulk form.

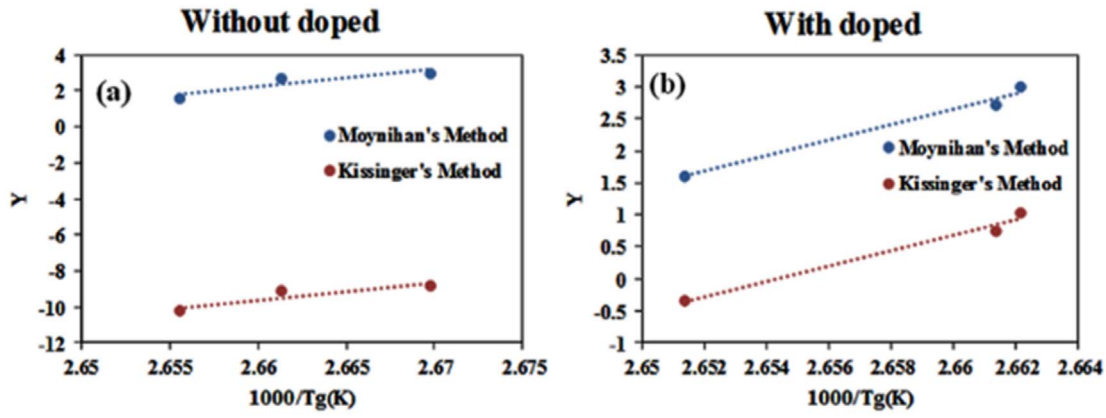

Figure 7. Plots of ln(β) and ln(β/Tg^2) against 103/Tg for (a) undoped $Ge_{22}As_{20}Se_{58}$ glass and (b) 3% Eu doped $Ge_{22}As_{20}Se_{58}$.

Furthermore, according to Moynihan's and Kissinger's models for the evaluation of activation energy (E_g) based on the glass transition kinetics and structural relaxation, the plots between lnβ versus $1/T_g$ corresponding to Moynihan's model and lnβ/Tg^2 versus $1/T_g$ (Kissinger's) were obtained for both pristine ChG and Eu-doped ChG glass [23–28]. These plots are displayed in figures 7(a)–(b), respectively.

The obtained Eg values of the materials are given in table 2. These values also showed that the thermal stability of ChG is greatly enhanced due to Eu doping due to its improved amorphous nature.

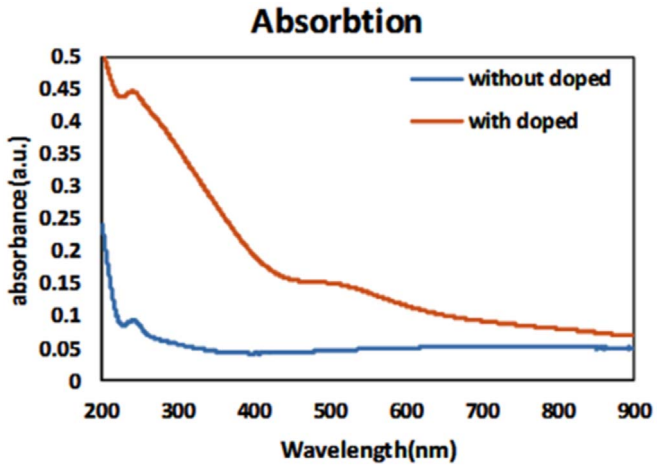

Figure 8. Absorbance spectrum of undoped and 3% Eu-doped $Ge_{22}As_{20}Se_{58}$ glass.

Table 2. Activation energy of glass transition for without and with doped glass.

Glass	E_g(KJ/mol)	
	Moynihan's Method	Kissinger's Method
$Ge_{22}As_{20}Se_{58}$	800.25	781.54
3% Eu^{3+} doped $Ge_{22}As_{20}Se_{58}$	1007.91	1001.67

4. Optical properties

4.1. Optical absorption spectra and bandgap estimations

The UV-visible absorption spectrum of the pristine and Eu doped-$Ge_{22}As_{20}Se_{58}$ glass is given in figure 8. It is observed from the spectra that the optical absorption properties of the doped ChG is significantly increased as compared to the undoped ChG. Notably, the absorption was enhanced in both UV (250–400 nm) as well as visible region (400–600 nm) of the spectrum.

This could be essentially attributed to Eu doping-induced formation of new 4 *f* energy levels in the optical bands of the host $Ge_{22}As_{20}Se_{58}$ glass, where it shows optical transitions at 393 nm ($^7F_0 \rightarrow {}^5L_6$), 464 nm ($^7F_0 \rightarrow {}^5D_2$), and 525 nm ($^7F_0 \rightarrow {}^5D_1$) [29]. The Judd-Ofelt theory does not show the first order transition of NIR photons corresponding to europium, which is because of the chalcogenide glass environment. As compared to the undoped $Ge_{22}As_{20}Se_{58}$ glass, the absorption spectrum of Eu doped $Ge_{22}As_{20}Se_{58}$ glass show some new optical transitions at 464 nm ($^7F_0 \rightarrow {}^5D_2$) and 525 nm ($^7F_0 \rightarrow {}^5D_1$). These absorption bands emerged due to Eu doping that created new optical transitions between the ground and excited states. Notably, these new absorption transitions take place from the ground level to the succeeding excited and thermal-populated states. However, the transition from $^7F_0$ to $^5D_1$ at 525 nm is found to be weak as compared to the other transitions from $^7F_0$ to $^5D_2$ and $^7F_0 \rightarrow {}^5L_6$ at 464 and 393 nm, respectively. This weak transition could be assigned to the partially allowed forbidden transition due to crystal-field transition. Similarly, no transitions in NIR region was observed due to their weaker optical transitions at higher wavelengths. The transition from $^7F_0$ to $^5D_2$ is induced by Eu-doping, which is due to the electric-dipole transition, and it is hyper-sensitive in nature. On the other hand, the $^7F_0$ to $^5D_1$ transition emerged based on the magnetic-dipole selection rule, and thereby, it possesses very less absorption intensity as compared to the $^7F_0$ to $^5D_2$ electric-dipole transition [30]. Furthermore, the blunt absorption profiles of both the doped and undoped ChG indicate their amorphous nature; however, the improved optical absorption for doped ChG could be ascribed to the presence of Eu^{3+} ions in the host material [31]. Generally, the optical properties of crystalline materials are governed by the valence band and conduction band with direct or indirect band gap structure, whereas, in amorphous materials, the optical properties are governed by different kinds of absorption edges with respect to the photon energy near the energy gaps [32]. Therefore, the study of the optical absorption characteristics of glass or amorphous materials could be one of the comprehensive tools to understand and predict their electronic band-structure [31]. Especially, the optical response of an amorphous material could be vigilantly modified upon doping. Accordingly, the band gap energy

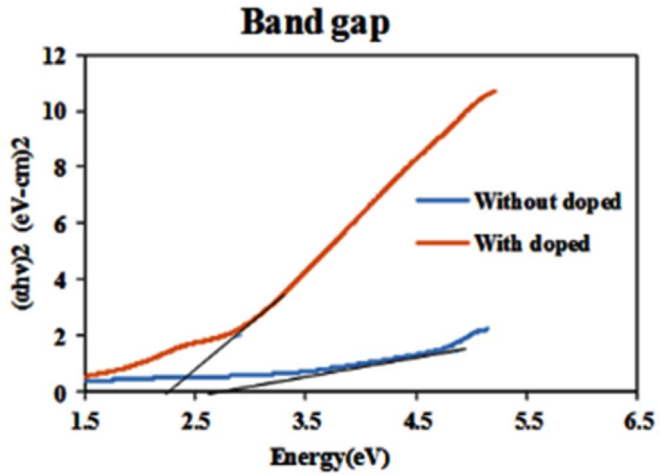

Figure 9. Estimation of band gap energy using Tauc plots of undoped and 3% Eu-doped $Ge_{22}As_{20}Se_{58}$ glass.

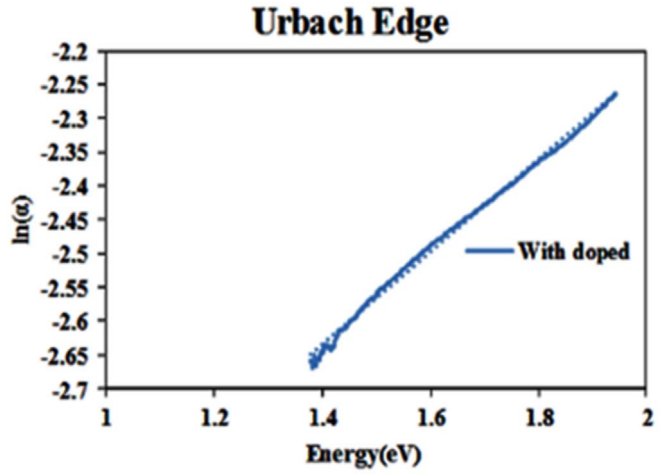

Figure 10. Urbach edge energy of 3% Eu-doped $Ge_{22}As_{20}Se_{58}$ glass.

of these synthesized doped and undoped ChG is estimated from their respective Tauc plots derived from their absorption spectra. The Tauc plot for the direct allowed transitions, i.e., $(\alpha h\nu)^2$ as a function of energy, was plotted, and the obtained plot is given in figure 9. It is observed that the estimated band gap energy for this direct-allowed transition is found to be 2.6 and 2.2 eV for the undoped and doped ChG, respectively. This decreased band gap energy for the doped ChG clearly indicates that there could be some structural disorders in the system that give rise to the different kinds of absorption edges due to doping as corroborated from the obtained absorption spectrum of the material.

The doping-induced structural disorders and defects can be analyzed using the concept of Urbach's edge or band tailing energy [31]. It is known that the localized short-range crystalline orders are interlinked into the long-range amorphous orders in the glass materials. Therefore, any induced disorders in the glass materials will also affect their Urbach's edge energy, and hence, the Urbach's energy was calculated by taking the reciprocal value of the slope of $\ln(\alpha)$ versus $h\nu$ plot as shown in figure 10. From the plot, the Urbach energy was estimated to be 4.35 and 3.59 eV for undoped and Eu-doped ChG, respectively. It is evident from the observed decreased Urbach's energy that Eu doping has led to the shifting of band edge position of the host $Ge_{22}As_{20}Se_{58}$ glass and improved their overall optical properties through amorphization. It is known that the increased interatomic spacings decreases the potential difference between the valence and conduction bands, which are eventually involve in the shifting of the band edge position, and thereby, it alters the band gap energy of the system as well. Moreover, the high electron affinity of Eu^{3+} ions is also involved in band structure modification,s and the grouping of the particles also leads to the reduction of band gap energy of the materials [33].

Table 3. Various physical parameters calculated from band gap energy.

Materials	E_g (eV)	n	ε_{∞}.	ε_0	$\frac{m_e^*}{m_0}$
$Ge_{22}As_{20}Se_{58}$	2.6	1.893	3.6	9.2	0.1833
$Ge_{22}As_{20}Se_{58}$(3% Eu^{3+}ions)	2.2	2.299	5.2	7.1	0.2002

4.2. Estimation of refractive index and dielectric constant

Moss relation is considered as one of more suitable models to assess the amorphous nature of the materials by correlating their refractive index and band gap energy, and it can be defined as n = 4.16–0.85 Eg [34, 35]. Similarly, the dielectric behavior of the materials validates their applications in high frequency optical transmission applications, which can be derived from the equation $\varepsilon_{\infty} = n^2$, and the static dielectric constant can be obtained from the equation $\varepsilon_0 - 33.26876 + 78.61805\, E_g - 45.70795\, E_g^2\, 8.32449\, E_g^3$ [35] Further, the electron effective mass of the crystalline and amorphous based semiconductor is also important as it depends upon the band gap energy of the material and can be estimated from the equation $\frac{m_e^*}{m_0}$ 5.17004–7.46699 E_g $+3.63286\, E_g^2 - 0.57525\, E_g^3$ [35]. The estimation of these values for pristine and Eu-doped $Ge_{22}As_{20}Se_{58}$ glass is given in table 3, where these obtained values for doped ChG clearly indicated that Eu doping enhanced the optoelectronic properties of the host $Ge_{22}As_{20}Se_{58}$ glass.

5. Conclusion

In conclusion, the commercial $Ge_{22}As_{20}Se_{58}$ glass was modified by doping with Eu^{3+} ions towards enhancing its amorphous nature, thereby to improve its structural, thermal and optical properties. Accordingly, the crystalline nature of pristine $Ge_{22}As_{20}Se_{58}$ glass was decreased with Eu doping, which was confirmed from the obtained XRD patterns of the samples. The Raman studies showed that Se in $Ge_{22}As_{20}Se_{58}$ glass was more influenced by Eu doping, which broke down the long-range crystalline networks into the short-range orders, and thereby, it improved the amorphous nature of the material. The obtained SEM and TEM images demonstrated evident changes in surface morphology and internal structure of the doped $Ge_{22}As_{20}Se_{58}$ glass. Further, the thermal studies using DSC revealed that Eu doping enhanced the thermal stability of glass, whereas the typical germanium lenses or chalcogenide lenses do not possess greater thermal stability, and therefore, they cause problems during the defocusing process in imaging. Similarly, the optical results showed that the optical absorption of the doped glass is got extended across the UV-visible region, and its band gap energy is also decreased. Overall, the obtained results in this study demonstrated that the developed synthesis strategy and Eu-doping are promising towards improving the amorphous, optical and thermal properties of $Ge_{22}As_{20}Se_{58}$ glasses towards their potential applications in thermal imaging.

Acknowledgments

Authors are thankful to IOE [6031] BHU for providing funds for chemicals.

Declarations

Conflict of interest

None.

Author contributions

AKS: Conceptualization, Methodology, HM: Writing- Original draft preparation, Writing- Reviewing and Editing; SKM: Conceptualization, Writing- Reviewing and Editing;-NM:, Editing.

Ethics approval

Not applicable.

Funding

This research did not receive any specific grant from funding agencies in the public, commercial, or not-for-profit sectors. AKS and HM is thankful to IOE (6031) BHU for financial support for chemicals.

ORCID iDs

Hirdeysh Mishra https://orcid.org/0000-0003-3734-2832

References

[1] Heo J and Chung W J 2014 Rare-earth-doped chalcogenide glass for lasers and amplifiers *Chalcogenide Glasses: Preparation Properties and Applications* (Elsevier: Woodhead Publishing Limited) 11 347–80
[2] Zhang X H, Guimond Y and Bellec Y 2003 Production of complex chalcogenide glass optics by molding for thermal imaging *J. Non. Cryst. Solids.* **326** 519–23
[3] Tikhomirov V K 1999 Photoinduced effects in undoped and rare-earth doped chalcogenide glasses *J. Non Cryst. Solids.* **256** 328–36
[4] Choi Y G 2007 Spatial distribution of rare-earth ions in Se-based chalcogenide glasses with or without Ga *J. Non. Cryst Solids.* **353** 1930–5
[5] Li G, Li L, Huang X, Tang J, Dai S, Wang G, Xu T and Jiao Q 2016 Er^{3+} doped and Er^{3+}/Pr^{3+} co-doped gallium-antimony-sulphur chalcogenide glasses for infrared applications *Opt Mat Exp.* **6** 3849–56
[6] Abdellaoui N *et al* 2018 Tb^{3+} doped $Ga_5Ge_{20}Sb_{10}Se_{65-x}Te_x$ (x = 0–37.5) chalcogenide glasses and fibers for MWIR and LWIR emissions *Opt Mat Exp.* **8** 2887–900
[7] Sujecki S 2018 Modelling and design of lanthanide ion-doped chalcogenide fiber lasers: Progress towards the Practical realization of the first MIR chalcogenide fiber laser *Fibers.* **6** 25
[8] Shiryaev V, Anashkina E and Karaksina E 2019 Experimental and Numerical Study of Emission Properties of Pr(3+)-Doped Ga(In)-Ge-As-Se Glass Fibers. *21st Int. Conf. on Transparent Optical Networks (ICTON-2019), Angers (France, 27 September 2019)* (IEEE) 1–4
[9] Churbanov M F, Denker B I, Galagan B I, Koltashev V V, Plotnichenko V G, Sverchkov S E, Sukhanov M V and Velmuzhov A P 2019 Peculiarities of 1.6–7.5 μm Pr^{3+} luminescence in $Ge_{36}Ga_5Se_{59}$ glass *Opt. Mat. Exp.* **9** 4154–64
[10] Starecki F, Louvet G, Ari J, Braud A, Doualan J L, Chahal R, Hafienne I, Boussard-Plédel C, Nazabal V and Camy P 2020 Dy^{3+} doped GaGeSbSe fiber long-wave infrared emission *J luminescence.* **218** 116853
[11] Gokhan K, Shams A M I, Erkan I, Kilicoglu O and Tekin H O 2021 A journey for exploration of Eu_2O_3 reinforcement effect on zinc-borate glasses: Synthesis, optical, physical and nuclear radiation shielding properties *Ceram. Int.* **47** 2572–3
[12] Naseer K A, Marimuthu K, Mahmoud K A and Sayyed M I 2021 Impact of Bi_2O_3 modifier concentration on barium–zincborate glasses: physical, structural, elastic, and radiation-shielding properties *Eur. Phys. J. Plus.* **136** 116
[13] Elliott S R 1991 Origin of the first sharp diffraction peak in the structure factor of covalent glasses *Phys. Rev. Lett.* **67** 711
[14] Kavetskyy T S, Shpotyuk O I and Boyko V T 2007 Void-species nanostructure of chalcogenide glasses studied with FSDP-related XRD *J Phy Chem Sol.* **68** 712–5
[15] Lin C, Rüssel C and Dai S 2018 Chalcogenide glass-ceramics: functional design and crystallization mechanism *Prog Mat Sci.* **93** 1–44
[16] Wei W H, Wang R P, Shen X, Fang L and Luther-Davies B 2013 Correlation between structural and physical properties in Ge–Sb–Se glasses *J Phy Chem.* **117** 16571–6
[17] Olivier M *et al* 2014 Structure, nonlinear properties, and photosensitivity of (GeSe 2) 100-x (Sb 2 Se 3) x glasses *Opt. Mater. Exp.* **4** 525–40
[18] Wang X *et al* 2012 Investigations of Ge–Te–AgI chalcogenide glass for far-infrared application *Spectrochim. Acta, Part A* **86** 586–9
[19] Ashraf S S, Zulfequar M and Uddin M 2018 Thermal analysis of Se-based chalcogenide glass *Rec Innovat Chem Eng.* **11** 172–8
[20] Lucas P, Coleman G J, Sen S, Cui S, Guimond Y, Calvez L, Boussard-Pledel C, Bureau B and Troles J 2019 Structural and chemical homogeneity of chalcogenide glass prepared by melt-rocking *J. Chem. Phys.* **150** 014505
[21] Chen R, Tian Y, Li B, Wang C, Jing X, Zhang J and Xu S 2016 Infrared fluorescence, energy transfer process and quantitative analysis of thulium-doped niobium silicate-germanate glass *Infrared Phy Technol.* **79** 191–7
[22] Lee J H *et al* 2016 Thermal properties of ternary Ge–Sb–Se chalcogenide glass for use in molded lens applications *J Non-Crystal Solids.* **431** 41–6
[23] Kasap S O and Juhasz C 1986 Kinematical transformations in amorphous selenium alloys used in xerography *J. Mater. Sci.* **21** 1329–40
[24] Larmagnac J P, Grenet J and Michon P 1981 Glass transition temperature dependence on heating rate and on ageing for amorphous selenium films *J Non-Crystal Solids.* **45** 157–68
[25] Moynihan C T, Easteal A J, Wilder J and Tucker J 1974 Dependence of the glass transition temperature on heating and cooling rate *J Phy Chem.* **78** 2673–7
[26] Abd El-Moiz A B, Afify N and Hafiz M M 1992 DTA studies on the crystallization of In_xSe_{1-x} chalcogenide glasses *Physica B: Condensed Matter* **182** 33–41
[27] Kissinger H E 1957 Reaction kinetics in differential thermal analysis *Analyt Chem.* **29** 1702–6
[28] Kissinger H E 1956 Variation of peak temperature with heating rate in differential thermal analysis *J. Res. Natl. Bur. Stand.* **57** 217–21
[29] Demesh M, Yasukevich A, Kisel V, Dunina E, Kornienko A, Dashkevich V, Orlovich V, Castellano-Hernández E, Kränkel C and Kuleshov N 2018 Spectroscopic properties and continuous-wave deep-red laser operation of Eu^{3+}-doped $LiYF_4$ *Optics Letters* Optical Society of America **43** 2364–7
[30] Manasa P and Jayasankar C K 2016 Luminescence and phonon side band analysis of Eu^{3+} doped lead fluorosilicate glasses *Opt. Mater.* **62** 139–45

[31] Naseer K A and Marimuthu K 2021 The impact of Er/Yb co-doping on the spectroscopic performance of bismuth borophosphate glasses for photonic applications *Vacuum* **183** 109788
[32] Urbach F 1953 The long-wavelength edge of photographic sensitivity and of the electronic absorption of solids *Phys. Rev.* **92** 1324
[33] Li L L, Hu J and Yang W 2001 Band gap variation of size and shape-controlled colloidal CdSe quantum rods *Nano Lett.* **1** 349–51
[34] Gupta V P and Ravindra N 1980 Comments on the moss formula *Infrared Phys. Technol.* **100** 715–9
[35] Ravindra N M, Ganapathy P and Choi J 2007 Energy gap–refractive index relations in semiconductors–An overview *Infrared Phys. Technol.* **50** 21–9